AFRL-RD-PS-
TP-2009-1011

AFRL-RD-PS-
TR-2009-1011

THE BALLOON RING: A HIGH-PERFORMANCE LOW-COST INSTRUMENTATION PLATFORM FOR MEASURING ATMOSPHERIC TURBULENCE PROFILES: POSTPRINT

Demos T. Kyrazis et al.

Air Force Research Laboratory
3550 Aberdeen Ave SE
Kirtland AFB, NM 87117

22 June 2009

Technical Paper

APPROVED FOR PUBLIC RELEASE; DISTRIBUTION IS UNLIMITED.

AIR FORCE RESEARCH LABORATORY
Directed Energy Directorate
3550 Aberdeen Ave SE
AIR FORCE MATERIEL COMMAND
KIRTLAND AIR FORCE BASE, NM 87117-5776

REPORT DOCUMENTATION PAGE

Form Approved
OMB No. 0704-0188

Public reporting burden for this collection of information is estimated to average 1 hour per response, including the time for reviewing instructions, searching existing data sources, gathering and maintaining the data needed, and completing and reviewing this collection of information. Send comments regarding this burden estimate or any other aspect of this collection of information, including suggestions for reducing this burden to Department of Defense, Washington Headquarters Services, Directorate for Information Operations and Reports (0704-0188), 1215 Jefferson Davis Highway, Suite 1204, Arlington, VA 22202-4302. Respondents should be aware that notwithstanding any other provision of law, no person shall be subject to any penalty for failing to comply with a collection of information if it does not display a currently valid OMB control number. **PLEASE DO NOT RETURN YOUR FORM TO THE ABOVE ADDRESS.**

1. REPORT DATE *(DD-MM-YYYY)*	2. REPORT TYPE	3. DATES COVERED *(From - To)*
23/06/2009	Technical Paper	June 23, 2009

4. TITLE AND SUBTITLE

The balloon ring: a high-performance low-cost instrumentation platform for measuring atmospheric turbulence profiles: Postprint

5a. CONTRACT NUMBER
N/A

5b. GRANT NUMBER

5c. PROGRAM ELEMENT NUMBER
N/A

6. AUTHOR(S)

Demos T. Kyrazis; Frank D. Eaton*; Lab Don G. Black; Wiley Black; Alastair Black

5d. PROJECT NUMBER
N/A

5e. TASK NUMBER
N/A

5f. WORK UNIT NUMBER
N/A

7. PERFORMING ORGANIZATION NAME(S) AND ADDRESS(ES)
Air Force Research Laboratory*
3550 Aberdeen Ave SE
Kirtland AFB, NM 87117-5776

8. PERFORMING ORGANIZATION REPORT NUMBER

9. SPONSORING / MONITORING AGENCY NAME(S) AND ADDRESS(ES)

Air Force Research Laboratory
3550 Aberdeen Ave SE
Kirtland AFB NM 87117-5776

10. SPONSOR/MONITOR'S ACRONYM(S)
AFRL/RDSE

11. SPONSOR/MONITOR'S REPORT NUMBER(S)
AFRL-RD-PS-TP-2009- 1011

12. DISTRIBUTION / AVAILABILITY STATEMENT

Approved for public release

13. SUPPLEMENTARY NOTES
Accepted for publication in the Optics and Photonics SPIE proceedings; San Diego California; August 4-6, 2009. Conference 7463 "Atmospheric Optics: Models, Measurements, and Target-in-the-Loop Propagation III." 377ABW-2009-0834, 1 Jul 2009. "GOVERNMENT PURPOSE RIGHTS"

14. ABSTRACT
Balloons, similar to those used for meteorological observations, are commonly used to carry a small instrumentation package for measuring optical turbulence in the atmosphere as a function of altitude. Two temperature sensors, one meter apart, measure a single point of the temperature structure function. The raw data is processed to provide the value of cr2, and the results transmitted to a ground receiving site. These data are converted to the index of refraction structure constant, Cn2. The validity of these measurements depend on the correctness of a number of assumptions. These include local isotropy of the turbulence and the existence of the Kolmogorov inertial sub range, and that the data is not contaminated by the wake of these ascending balloons. A variety of experiments on other platforms, and in the laboratory, demonstrate that the assumptions upon which these balloon measurements are made are not valid for a large percentage of the flights. In order to collect data whose interpretation did not require preconceived assumptions, the balloon ring instrumentation system was developed. The ring is 28.5 meters in diameter, with a cross-sectional diameter is 14 cm. The ring is hung just below the balloon, so that the wake goes through the center of the ring, and the sensors are mounted tangent to the circumference of the ring,.

15. SUBJECT TERMS
Balloon Measurements; Optical Turbulence; Atmospheric Turbulence

16. SECURITY CLASSIFICATION OF:			17. LIMITATION OF ABSTRACT	18. NUMBER OF PAGES	19a. NAME OF RESPONSIBLE PERSON
					Frank Eaton
a. REPORT	b. ABSTRACT	c. THIS PAGE			19b. TELEPHONE NUMBER *(include area code)*
Unclassified	Unclassified	Unclassified	SAR	16	505-853-1091

Standard Form 298 (Rev. 8-98)
Prescribed by ANSI Std. 239.18

This page is intentionally left blank.

The balloon ring: a high-performance low-cost instrumentation platform for measuring atmospheric turbulence profiles

Demos T. Kyrazis[a], Frank D. Eaton[b], Lab Don G. Black[c], Wiley Black[c], Alastair Black[a]
[a] R-Cubed, Inc., 1028 Tramway Lane, NE, Albuquerque, NM 87122;
[b] Air Force Research Laboratory, Kirtland AFB, NM;
[c] Ridgeline LLC, 63 Otero Rd., Los Lunas, NM, 87031

ABSTRACT

Balloons, similar to those used for meteorological observations, are commonly used to carry a small instrumentation package for measuring optical turbulence in the atmosphere as a function of altitude. Two temperature sensors, one meter apart, measure a single point of the temperature structure function. The raw data is processed to provided the value of C_T^2, and the results transmitted to a ground receiving site. These data are converted to the index of refraction structure constant, C_n^2. The validity of these measurements depend on the correctness of a number of assumptions. These include local isotropy of the turbulence and the existence of the Kolmogorov inertial subrange, and that the data is not contaminated by the wake of the ascending balloon. A variety of experiments on other platforms, and in the laboratory, demonstrate that the assumptions upon which these balloon measurements are made are not valid for a large percentage of the flights. In order to collect data whose interpretation did not require preconceived assumptions, the balloon ring instrumentation system was developed. The ring is 28.5 meters in diameter, with a cross-sectional diameter is 14 cm. The ring is hung just below the balloon, so that the wake goes through the center of the ring, and the sensors are mounted tangent to the circumference of the ring. The raw data is transmitted to the ground with a bandwidth extending to 1.25 kHz. A sample of the measurements taken during a flight at Vandenberg Air Force Base, California are presented.

Keywords: balloon measurements, optical turbulence, atmospheric turbulence

1.0 THE MEASUREMENT OF OPTICAL TURBULENCE WITH FREE BALLOONS

1.1 Description of the measurement technique.

The majority of optical turbulence measurements are made by free balloons similar to those used for weather observations using radiosondes. Typically, the measurements are made with two temperature sensors, with one meter separation between them. The sensor package is mounted below the balloon at the end of a long tether, typically 50 to 100 meters in length. A sketch of the balloon and instrumentation package is shown in Figure 1. Note that package swings as pendulum with a period of 15 to 20 seconds, normally tracing an elliptical path. The boundary of the wake is shown extending below the balloon. Depending on the width of the wake at the end of the tether, the sensors could be swinging in and out of the wake, or they could be totally immersed in the wake. However, if there is sufficient wind shear between the balloon and the sensors, then it is possible for the sensors to clear the wake and actually measure properties of the atmosphere.

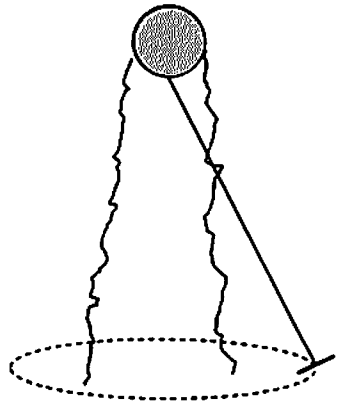

Figure 1. Balloon with sensor package.

In considering the effect of the wake, 100 meters below a balloon of 2 meters

diameter appears to be sufficiently far that the wake would have little effect. However, from a fluid dynamic viewpoint, the sensors are only 50 balloon diameters below, and can get as close as 10 to 15 diameter at higher altitudes as the balloon expands. In laboratory experiments, the thermal wake is detectable at over 1000 diameters downstream[1].

The function of optical interest is the structure function, D(r), from which the propagation phase screens can be constructed. This can be measured using two temperature probes that are separated by a variable distance, r. If the separation distance, r, is much smaller than the turbulence outer scale, and greater than the inner scale, then the following formula, by Tatarski[2], can be used to measure the value of the structure constant, C_T^2, by measuring the temperature, T, at a location x in space.

$$D(r) = \left\langle \{T(x) - T(x+r)\}^2 \right\rangle = C_T^{\,2} \cdot r^p \qquad (0 < p < 2) \qquad (1)$$

Note that dimension of C_T^2 is dependent on the value of the exponent, p. Tatarski also showed that the power law describing the Power Spectral Density (PSD) of the turbulence is $-(1 + p)$.

The success of the above described balloon measurement technique is totally dependent on knowing the characteristics of the turbulence being measured. Two assumptions are made. The first is that the outer scale of the turbulence is much greater than the scale of the optical systems being considered. The second is that local isotropy exists, and that the measurements are made within the Kolmogorov inertial subrange. In that case, the value of p is 2/3. As a result, it is only necessary to measure the two temperatures at a single value of r, typically one meter. However, recent literature has shown that these assumptions are often incorrect, and that balloon wake interference is a problem with the above measurement technique.

Tiefenau[3] have measured the wake effects of an ascending balloon, and Barat point out that wake contamination must be considered, and that the data has to be examined to identify those times when the sensors are in the wake. Koop had pointed out that experiments had shown that the thermal wake behind a blunt body is detectable over 1000 diameters behind the body. In the balloon measurements, the balloon diameter is approximately 1 meter. Thus the sensors are approximately 100 diameters below the balloon at launch, and approach 20 diameters at the higher altitudes as the balloon expands. Dalaudier et al and Gurvich point out nonisotropy, layering, and steep temperature gradients in the atmosphere, while Kyrazis et al report of aircraft measurements showing extended distance of non-Kolmogorov turbulence, and outer scales of less than 1 meter.

1.2 Improving the measurement technique.

The two basic problems discussed in the previous section are

(1) how to guarantee that the sensors are out of the balloon wake;
(2) how to measure the desired turbulence properties without making assumptions about other turbulence properties.

The balloon ring and its instrumentation system solve both those problems.

1.2.1 Discussion of the balloon wake problem.

We will first address the problem of the wake behind the balloon by examining the CLEAR I model of atmospheric optical turbulence that was developed by Beland at the Air Force Geophysics Lab. This was chosen for two reasons. This model is used by the Air Force's Airborne Laser Aircraft, and more detailed data from the balloon launches was available for examination.

The CLEAR I model provides a value of the index of refraction structure constant, C_n^2, as a function of altitude under the assumption that atmospheric temperature turbulence is Kolmogorov. However, the quantity that is actually measured is the temperature structure constant, C_T^2. To examine the nature of the measured quantity, the CLEAR I model was converted back to a plot of C_T^2 as a function of altitude by using the US Standard Atmosphere. When that was done, it

was noted that the value of C_T^2 was almost constant in the stratosphere, as seen in Figure 2. This was suspicious, but it was consistent with the idea of the probe being immersed in the balloon wake[4]. More significantly, there was an abrupt change in slope of the function around 10 km altitude. This prompted a calculation of the balloon Reynolds number as a function of altitude, and it was found that the discontinuity in the slope occurred at a Reynolds number around 400,000, which is the critical Reynolds number for the flow around a sphere. Normally, the transition is more abrupt. Since the CLEAR I model is the average of many flights, the differing atmospheric conditions for each flight would smear out the altitude of transition.

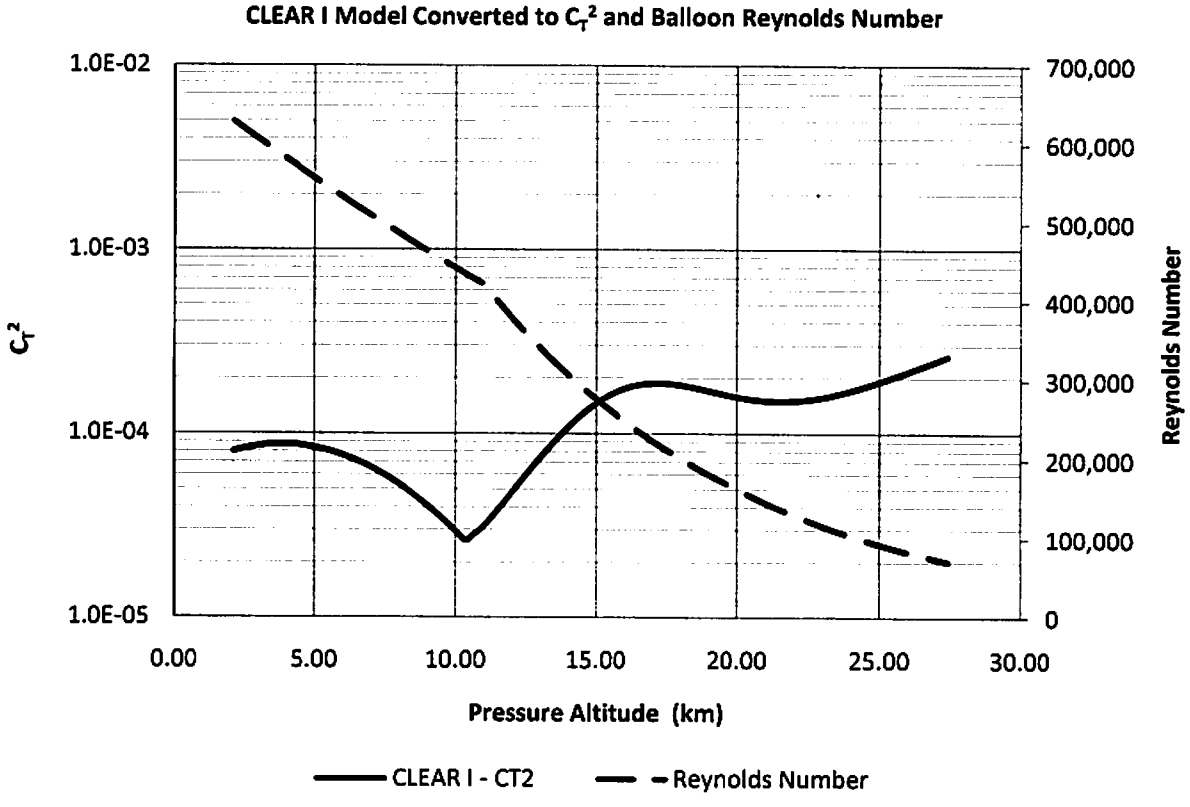

Fig. 2. Comparison of CLEAR I model with lines of constant C_T^2 that are converted to C_n^2 as a function of altitude. Note plot of balloon Reynolds number, which changes primarily as a result of balloon diameter and kinematic viscosity.

The nature of the flow around a body of a given shape depends upon the Reynolds number. Thus, if two bodies are geometrically similar, but are of different size , then the flow patterns will be similar providing the corresponding Reynolds numbers are equal. The Reynolds number can be considered to be the ratio of inertial forces to viscous forces in a fluid. It is defined by equation 2.

$$Re = UD/\nu \tag{2}$$

Where

U = The velocity of the body through the fluid
D = A characteristic length of the body, which for a sphere is the diameter
ν = the kinematic viscosity of the fluid.

The sphere, being a blunt body, generates a large wake behind it, and the nature of the wake depends on the Reynolds number. For the class of balloon experiments being discussed, the Reynolds number can vary 50,000 to 1,000,000 depending on altitude and size of the balloon. For a sphere, the nature of the wake changes dramatically at the critical number of approximately 400,000. Above the critical Reynolds number, the drag coefficient of the sphere decreases by factor of 6. The reason for the drag reduction is that the size of the wake abruptly becomes smaller above the critical Reynolds number. The cause of the change in wake size depends on where the flow separates from the surface of the sphere[5] as is illustrated in Figure 3.

(a) (b)

Fig. 3. Wake behind a sphere for Reynolds below and above the critical Reynolds number of 400,000. (a) Flow separates about 80° from stagnation point below critical Reynolds number, resulting in large wake and high drag coefficient. (b) Flow separates at approximately 120°, resulting in smaller wake and lower drag coefficient.

The possibility of wake contamination was carefully considered Barat[6], Azouit[7], and others. A major consideration was whether the wake diameter at the location of the sensors suspended below the balloon was sufficiently small that the prevailing wind shears in the atmosphere would keep the sensors out of the wake. To estimate the wake diameter, Barat used published measurements of the wake behind a disk, and concluded that the wake diameter would be twice the diameter of the balloon. This proved to a useful rule for determining the distance below the balloon for the sensors, in order to utilize the atmospheric wind shear to minimize wake contamination of the measurements. It turned out that this was a useful rule for the balloon launches of Barat and Dalaudier[8] since they used similar balloons, but completely wrong for the launches of Azouit.

One has to be careful how one applies wake measurements made in the laboratory to tests made in the field. The wake generated by a disk has a well defined, fixed separation line. On the other hand, the separation line generated by a cylinder or a sphere is variable both in time and space. Consequently, the wake of the disk would have very different characteristics from that of a cylinder or sphere. The Barat balloon was a zero pressure balloon with a volume of 10,000 cubic meters. At launch the bubble of He or H_2 form a hemisphere at the top, 3 m in diameter. The rest of the balloon formed a cone from the hemisphere and coming to a point 38 meters below the hemisphere. This is a highly streamlined body, therefore the flow will not separate until close to the point of the cone. Hence, the wake will be much smaller than the diameter of the balloon. As the balloon rises, the hemispherical portion will get larger, the cone angle will become steeper, and the separation will occur much earlier. At 31 km altitude the shape of the balloon is completely spherical with a diameter of 26 m. The wake will have very different characteristics, and it will diverge much more rapidly. For a very large percentage of the flight profile, the assumption of a wake diameter that is twice the balloon diameter would be a very conservative rule of thumb.

For the examination of balloon wake behind a sphere, we will use the conditions published by Azouit, referred to earlier. At launch the balloon was sphere with a diameter of 1.6 m. By the time it reached an altitude of 20 km, its diameter expanded to 4 m. The instrumentation package was at the end of a 50 m tether. The balloon diameter at intermediate

attitudes can be easily calculated. The wake behind a sphere has been well studied, and we will use the results published by Wu[9] to calculate the wake diameter at the end of a 50 m and a 100 m tether. The edge of the wake is taken at the nondimensional radius of 3. Note that this boundary only determines the diameter of the core of the wake, and does not include the turbulence intermittency region that surrounds the wake.

The results of calculating the wake diameter for different altitudes are presented in Table 1. For each altitude, the balloon diameter is given, as well as the wake diameter in meters for each tether length. The wake width and the tether length are then nondimensionalized in terms of balloon diameters. It should be noted that at no time is the wake width only 2 diameters as suggested by Barat. Also note that the ends of the tethers are fluid dynamically quite close to the balloon.

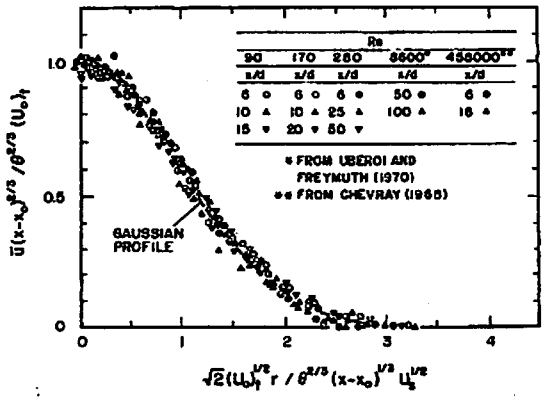

Fig. 5 Correlation of radial profiles of mean streamwise velocities in the turbulent wake region.

Fig. 4. Self preserving turbulent velocity profile for wake behind a sphere. Velocity and radius axes are nondimension-alized. The above data cover the Reynolds number range of interest to the current

Table 1. Balloon wake characteristics at 50 and 100 meters below balloon.

		Wake diameter (m)		Wake width (diameters)		Diameters below	
Pressure altitude (km)	Balloon diameter (m)	50 m	100 m	50 m	100 m	50 m	100 m
0	1.600	9.267	11.681	5.792	7.300	31.250	62.500
5	1.896	10.655	13.432	5.621	7.086	26.378	52.756
10	2.297	14.972	18.899	6.517	8.200	21.765	43.530
15	2.952	18.363	23.192	6.221	7.857	16.939	33.878
20	3.827	22.063	27.886	5.766	7.288	13.067	26.133
25	4.965	23.378	29.576	4.709	5.957	10.071	20.141

1.2.2 Solution to the balloon wake problem.

Various attempts to solve the balloon wake problem have been tried, while keeping the experiment under the same category as weather balloons under the the Federal Air Regulations. If this isn't done, the equipment weights and costs skyrocket as well needing to be under the jurisdiction of Air Traffic Control. Techniques that have been successful with large balloons, have been difficult to implement with the small balloons, in part, because of the restrictions imposed by regulation.

If we ask the question "when is the wake the smallest?", the answer is when the flow first separates from the balloon surface. Perhaps the problem of keeping the sensors out of the wake would be most easily solved if the sensors could be mounted very close to the balloon. One way of doing this, without having the wake touch any part of the structure, is by using a torus whose diameter is larger than the largest attained diameter of the balloon. The torus is then suspended immediately below the balloon. Thus, the wake goes through the central, open part, of the torus, and the instrumentation

and sensors are mounted on the circumference. Hence, the name balloon ring. A photo of the balloon ring is shown in Figure 5.

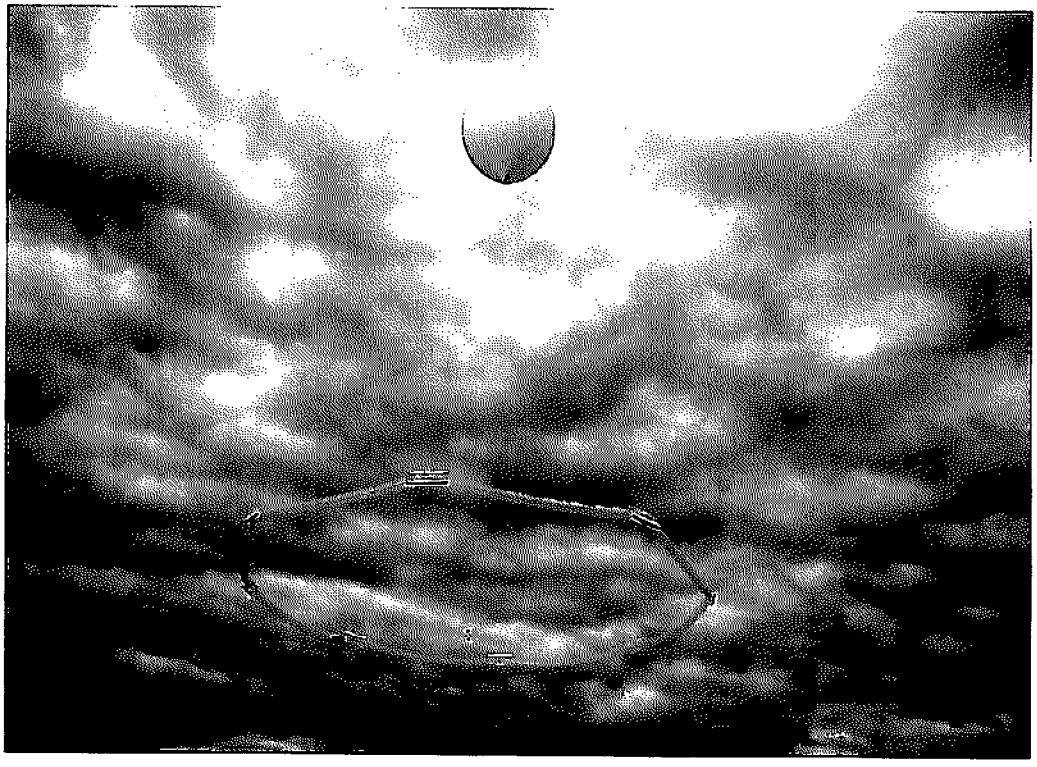

Fig. 5. Test flight of balloon ring without instrumentation.

Before breaking at an altitude of 24 km, the balloon diameter reaches 6 m. Therefore, the diameter of the balloon ring was set to 9 m. The ring is constructed of polyethylene tubing with a thickness of 0.006 in. (152.4 μm). It is inflated to a gage pressure of 2.25 psi (15,513 Pa), and a pressure relief valve maintains the pressure difference as the ring ascends. The cross-sectional diameter of the ring is 5.5 in. (14 cm). The instrumentation platform is 3 m long and 5 cm wide, which is mounted to one of the corner pieces, and tangent to the ring.

The most surprising of the balloon flights is the extreme stability of the ring as the balloon ascends. There is no perceptible rotation about any axis, nor is there any pendulum motion.

1.2.3 Measuring turbulence properties.

There is only one way to measure the turbulence properties without invoking some turbulence model to interpret the measurements. The raw data must be transmitted to the ground with sufficient bandwidth to provide a true picture of the turbulence phenomena. That is what the balloon ring instrumentation system accomplishes. One of the system requirements was to measure the inner scale down to 5 mm at normal ascent speeds of around 5 m/sec. This sets the frequency bandwidth requirements.

Six sensors are distributed along the instrumentation platform in order measure the horizontal structure function. The temperature sensors are made of 1 μm diameter platinum wire, with a reference resistance at 273.15 K of 500 Ω. The bias current is limited to 400 μa in order to reduce self heating errors. The wires have frequency response of 3 kHz. They are surprisingly rugged and have survived at speeds as high as 70 mph (31 m/sec) in clear air, and 26 mph (11.6 m/sec) in clouds. Each sensor has its own signal conditioning amplifier and digitizer, and system frequency response is from DC

to 1.2 kHz with a maximum sampling rate of 3.125 kilosamples per second. Any of the temperature sensor stations can be converted a velocity measurement by simply the analog signal conditioner circuit board.

The digital data from each sensor is collected by the telemetry formatter, which then drives the telemetry transmitter with biphase-L modulation at 500 kilobits/sec. At the ground station, a decommutator accepts the video output of the telemetry receiver and stores the data on a laptop computer as a binary file. While the data is being received, the sensor outputs can be view either graphically or numerically. The main components of the instrumentation system are illustrated in Fig. 6.

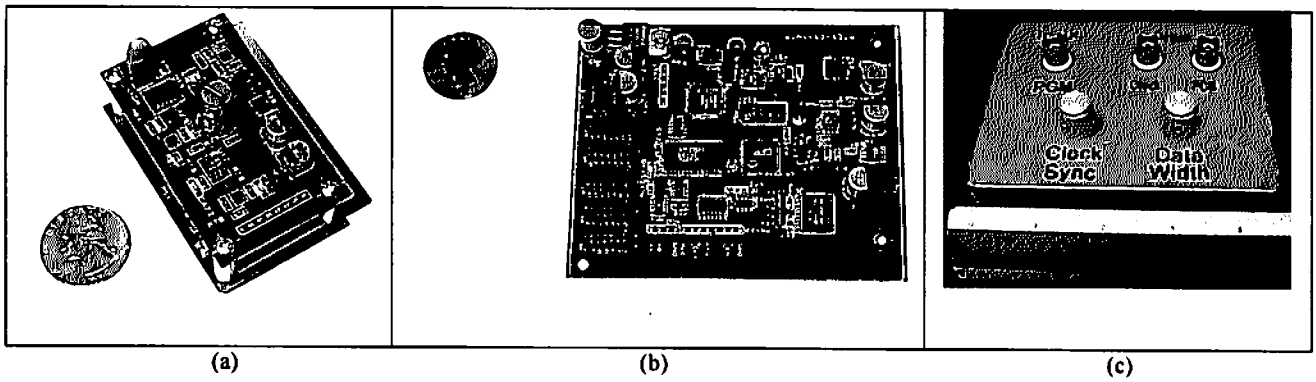

(a) (b) (c)

Fig. 6. Main components of instrumentation system. (a) Analog signal conditioner and digitizer. (b) Formatter. (c) Decommutator.

2.0 Optical turbulence measurements taken at Vandenberg AFB

Optical turbulence measurements were made by the balloon ring system at Vandenberg AFB, CA on 14 June 2007. These measurements were made simultaneously with 50 MHz wind profiler radar also located at Vandenberg. At the time of launch, the marine inversion layer had moved in, resulting in a thick fog layer. The balloon was launched through the fog at 08:27 PDT (15:27 Z) and did not clear the fog until it reached an altitude of 0.3 km. Thermal turbulence measurements were made over a 77 minute time period, covering a pressure altitude range of 0.3 to 23.5 km The temperature as a function of pressure altitude is plotted in Fig. 7. Note that there is considerable structure within the profiles.

At first the data was analyzed by breaking up the altitude range into 57 segments, each of which were 79.609 seconds long. The power spectral density (PSD) of each segment was calculated by dividing the each segment into 9 subsegments of 8.845 seconds in length. The PSD of each subsegment was calculated using a Hanning window, and the PSD's averaged. These operations for each segment was done in the time domain, and the conversion of the segment PSD to special frequency, i.e., wavenumber space, was accomplished by using the average ascent velocity for each segment. A PSD from the troposphere and the stratosphere are shown in Fig. 8. Note that the Fig. 8(a) appears to be very close representing an inertial subrange, and Fig. 8(b) shows no behavior resembling a Kolmogorov spectrum. Note also the flattening of the spectrum in Fig. 8(b), indicating a outer scale of less than a meter. The logarithmic slope of all 57 segments is plotted in Fig. 9. Note that even in the troposphere, most of the turbulence does not follow Kolmogorov theory.

Since having the raw data available allows us to perform a variety of analyses, then is C_n^2 the information that should be extracted from the data. The function of interest for optical propagation calculation is the structure function, D(r). C_n^2 is used to construct the structure function from Eq. (1). But, with the raw data available, it is actually easier to calculate the true structure function , and it relieves us from dependence on theoretical models. Two steps are involved in the calculation. The first is to calculate the autocorrelation function, $\Phi(r)$. This can be easily and quickly calculated by use of the Fast Fourier Transform (FFT). Plotting the autocorrelation function can be very informative because it separates the

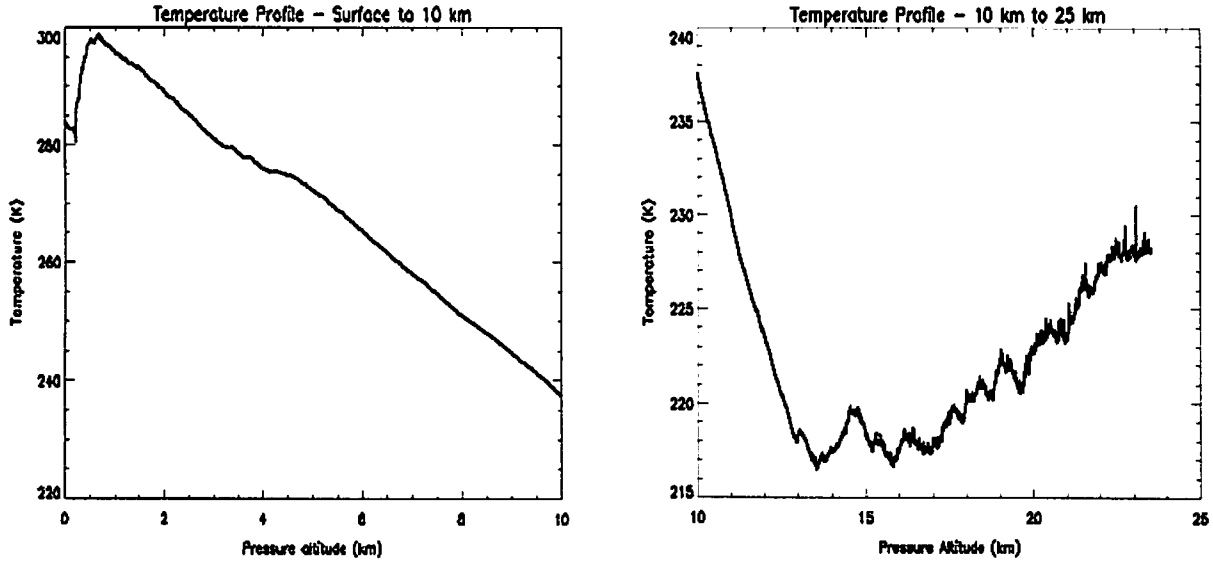

Fig. 7. Atmospheric temperature as function of pressure altitude.

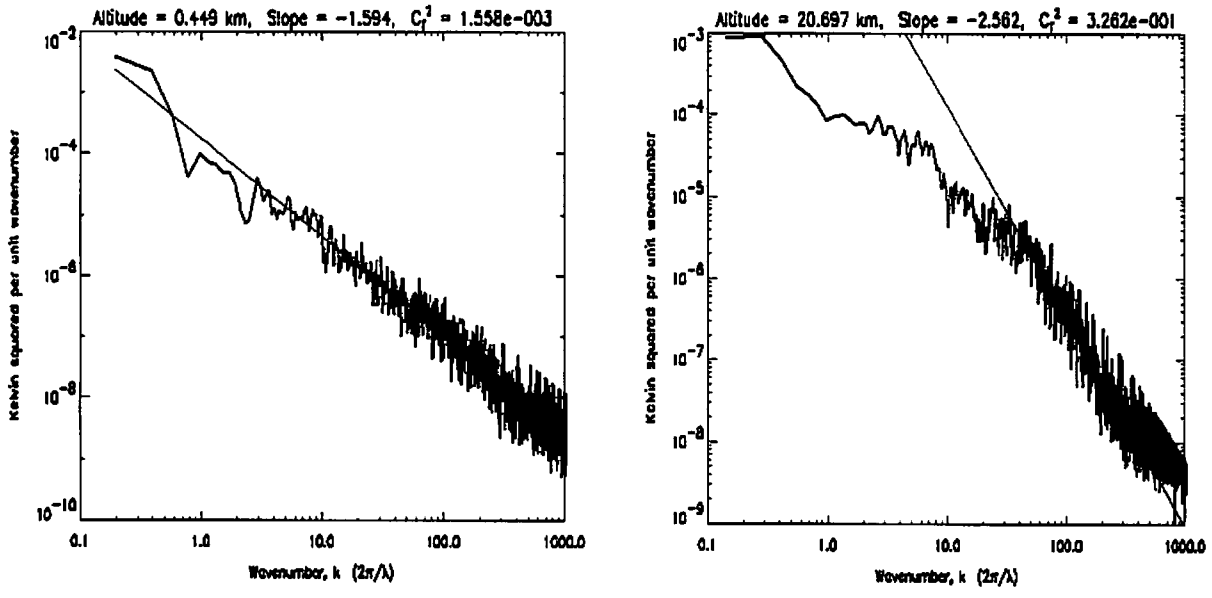

(a) (b)

Fig. 8. Sample of PSD's from the troposphere (a) and the stratosphere (b).

truly random fluctuations from other phenomena, such as large scale oscillations due to gravity waves. In addition, it allows a quick estimate of the outer scale. The structure function can then be calculated from the autocorrelation function by simple algebraic manipulation. The autocorrelation function is simply the temperature cross term in Eq. (1), i.e.,

(2)

In terms of the autocorrelation function, D(r) simply becomes

$$D(r) = 2\{\emptyset(0) - \emptyset(r)\} \qquad (3)$$

It would be interesting to observe the behavior of the structure function at a much finer scale than has been discussed so far. Since each segment was divided into 9 subsegments for the calculation of the segment PSD, we will now examine the properties of the subsegment structure functions.

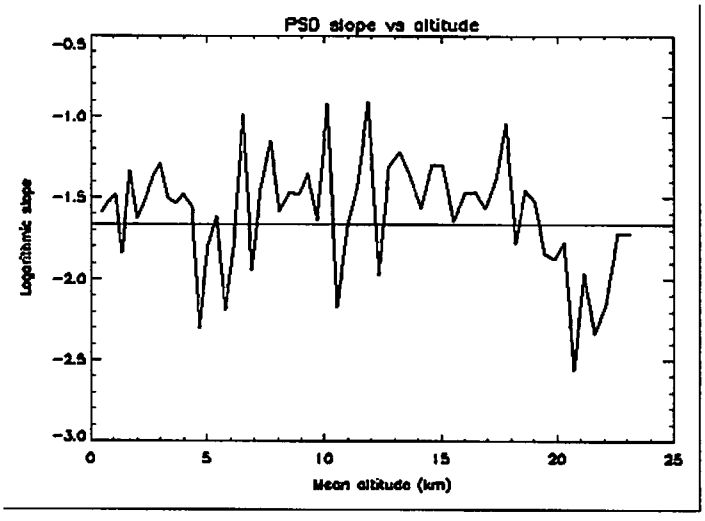

Fig. 9. Logarithmic slope of all 57 segments of the atmosphere. The horizontal line the Kolmogorov slope.

The segment just below the tropopause was chosen for further examination. The temperature profile is shown in Fig. 10(a). The autocorrelation function for this segment is plotted in 10(b). Note that there is a narrow spike at the origin of autocorrelation function. This is the part that contains energy of the random temperature fluctuations. The rest of the functions is basically uncorrelated. For other segments, both in the troposphere and in the stratosphere, we often observe large scale oscillations of the order of 100 meters, or more, between peaks.

The structure function for the segment is plotted in Fig. 10(c), and was calculated from the autocorrelation function of Fig. 10(b). The red line represents the $r^{2/3}$ power law for a Kolmogorov turbulence. The actual power law is p = 1. Note that the structure function flattens out at 3 meters reparation distance. This is the distance where the temperature fluctuations are no longer correlated. These short correlation distances occur quite often over the whole altitude range between 0.3 to 23.5 km. These short correlation lengths were also observed in high altitude aircraft measurements along a horizontal path[10].

The structure functions associated with the 9 subsegments are plotted in Fig. 10(d). Each of the subsegment structure functions is color code to the temperature profile in 10(a). The subsegments are about 35 to 40 meters long. The first thing that stands out is that there appears to be a layer bounded by the strong inversion at 13 km altitude and the tropopause at the other end. Inside the layer, the temperature turbulence is weak and approximately 2 to 10% of the strength at the layer boundaries. This is not a rare phenomenon, and occurs at all altitude ranges.

At the suggestion of Prof. Nastrom, a single 3.17 km, low altitude segment was analyzed. The results of this analysis leads to question as to the proper way to analyze the data. Fig. 11(a) is a plot of the segment PSD, calculated as a single PSD from the whole 3.17 km segment without any averaging. The spread of the spectrum is consistent with what would be expected from a random time function without any averaging of the PSD's[11]. The PSD was calculated using a Hanning window. Because of the large variation in balloon ascent rate over this large altitude range, the calculations were not spatial units.

The spread of the PSD is quite large, which leads to the question of how to best determine the power law of the PSD. We utilize two methods for determining spectral power law over the frequency range between 10 Hz and 1 kHz. The first is to determine the slope of a linear fit on the log-log plot. This logarithmic slope is the usual way for determining the PSD power law. This appears as an orange line in Fig. 11(a). The other method is to fit power law in physical space instead of

log space. This can take as long as 5 minutes compared to less than 1 second when the fit is done in log space. The physical space fit is shown as a red line.

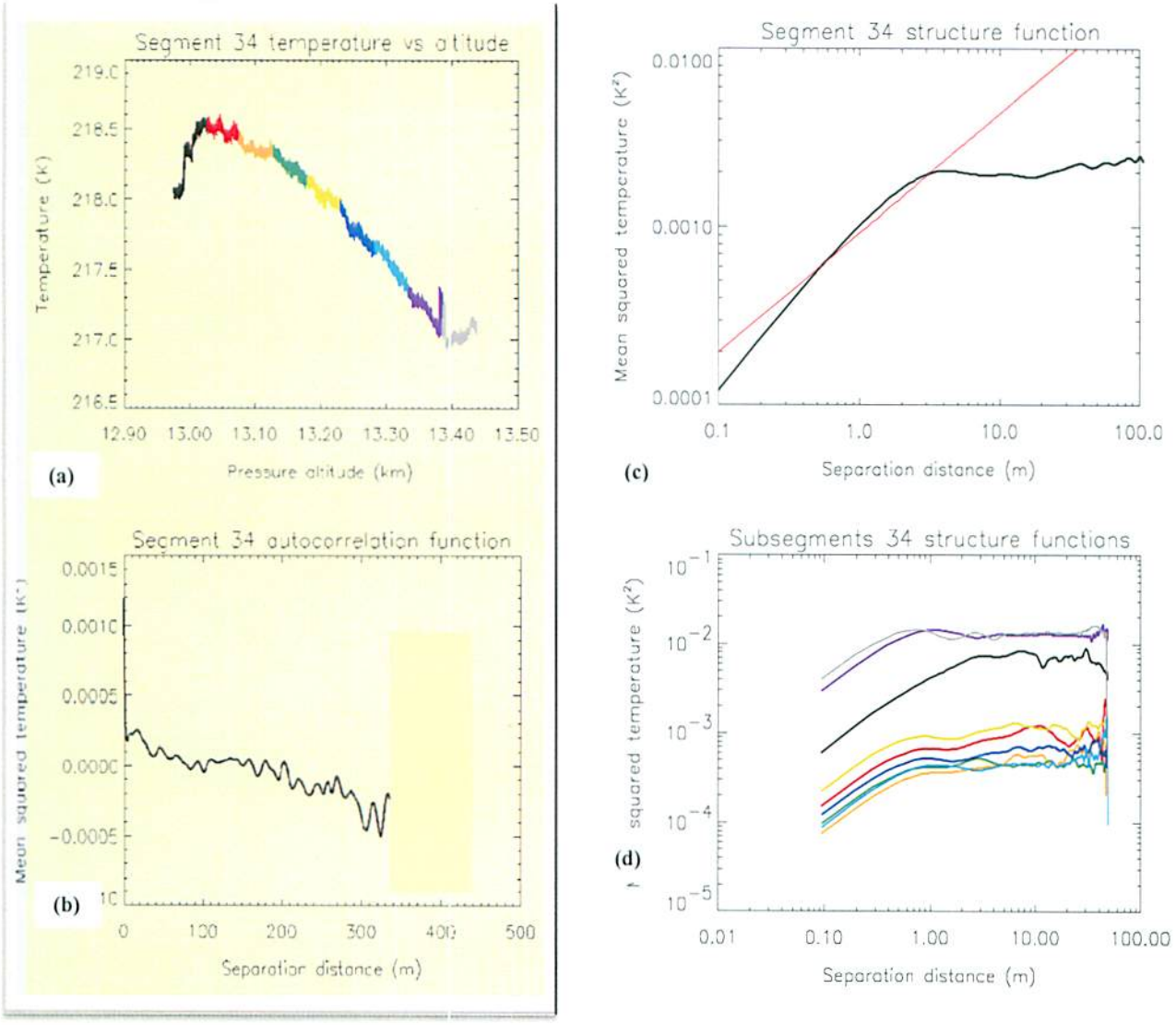

Fig. 10. Detailed analysis of segment 34. (a) Atmospheric temperature for the altitude shown. (b) The autocorrelation function of the temperature fluctuation in (a). (c) The structure function of (a) calculated from (b). (d) The structure functions of each of the 9 subsegments of (a).

The question then is which is the correct power law. This is answered by directly calculating the structure function from the time series, without resorting to the PSD. The structure function was calculated utilizing two different methods. The first was through the two step process of first calculating the autocorrelation function utilizing the FFT, and then the structure function from the autocorrelation function. This took less than one second to calculate. The second method was to calculate the structure function by direct application of Eq. (1). This took over an hour. The two structure functions are plotted in Fig. 11(b). The black is calculated by the first method ,and the green line by the second method. There no significant difference in results between the two methods.

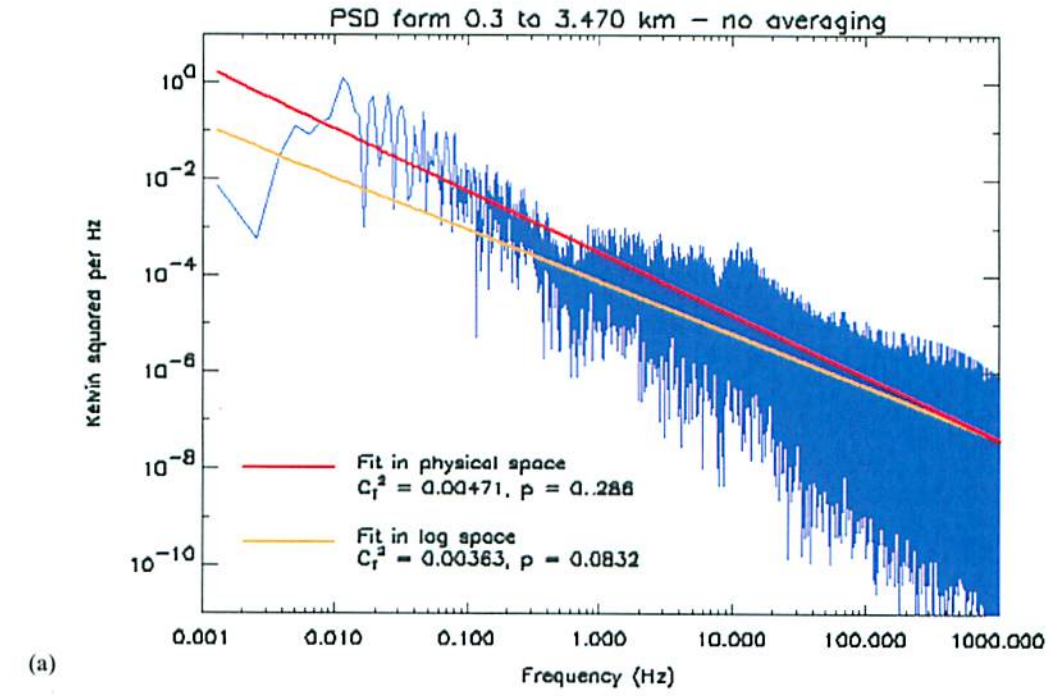

(a)

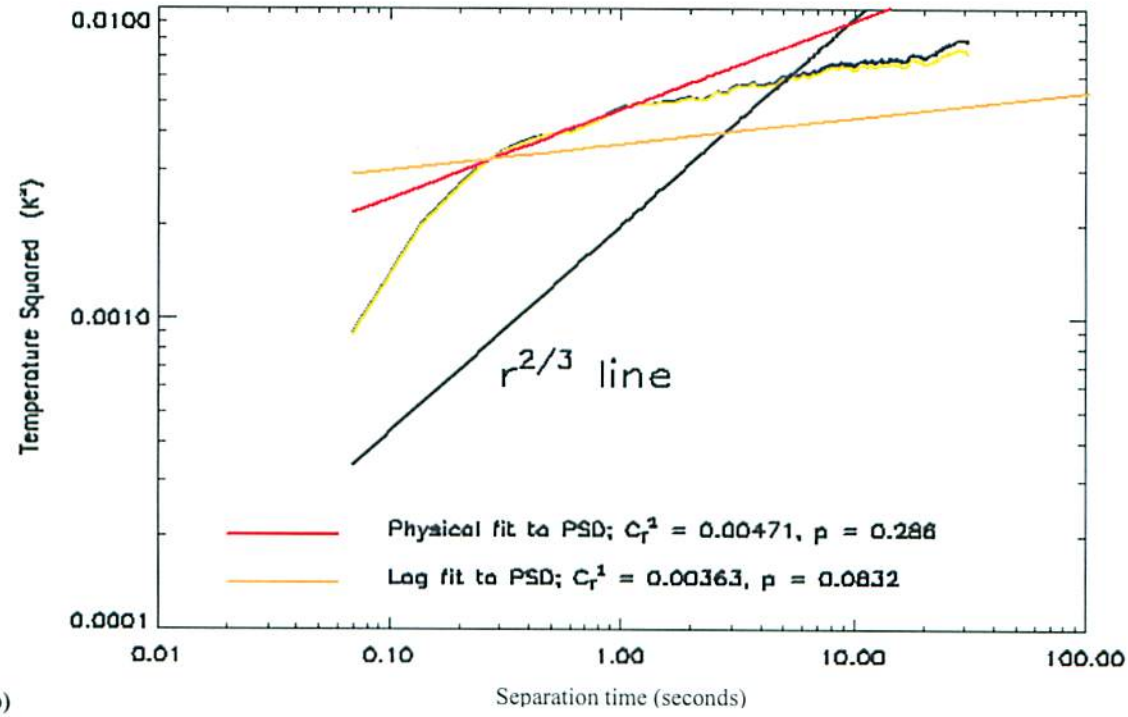

(b)

Fig. 11. Analysis a single 3.17 km long segment ranging from 0.3 to 3.470 km pressure altitude. (a) PSD of segment with no averaging. (b) Structure function calculated directly from time series, power laws derived from PSD.

Finally, we plot the structure functions derived from the PSD. The red line corresponds to the PSD fit in physical space. Note that it falls on top of the structure function. The orange line is from the fit in log space, Here we have no correlation whatsoever.

3.0 CONCLUSIONS

The balloon ring is a highly stable platform that avoids the problem of balloon wake contamination of the measurements. Early attempts to measure atmospheric optical turbulence by "weather" balloons were constricted by weight and density restrictions imposed by Federal Air Regulations (FAR). Modern electronic technology allows us to dramatically upgrade our measurement capability while still meeting the FAR's.

The balloon ring data has shown that varies significantly from the assumptions derived from Kolmogorov theory. In addition, the predominance short correlation lengths has a significant effect on optical propagation, and shows that the parameter, C_n^2 is insufficient to correctly describe the optical effects of the atmosphere.

We now have the capability, in a light weight package, to directly calculate the function of optical interest, i.e., the structure function. In addition, very high spatial resolution measurements can be made since the atmosphere is sampled every 320 μsec,

---

[1] Koop, personal communication.
[2] Tatarski, V. I. , "Wave propagation in a turbulent medium", Dover Publications, Inc. 1961.
[3] Tiefenau, H. K. E. and Gebbeken, A. , "Influence of meteorological balloons on temperature measurements with radiosondes: nighttime cooling and daylight heating, "Jour. of Atmospheric and Oceanic Technology," 6, 36-43.
[4] Sphere wake temperature paper. Gibson-8
[5] Schlichting
[6] Barat
[7] Azouit & Vernon
[8] Dalaudier
[9] Wu
[10] Wissler
[11] Blackman & Tukey

DISTRIBUTION LIST

DTIC/OCP
8725 John J. Kingman Rd, Suite 0944
Ft Belvoir, VA 22060-6218 1 cy

AFRL/RVIL
Kirtland AFB, NM 87117-5776 2 cy

Frank Eaton
Official Record Copy
AFRL/RDS 1 cy